Available online at www.sciencedirect.com
SCIENCE DIRECT
Journal of the European Ceramic Society 26 (2006) 49–58
www.elsevier.com/locate/jeurceramsoc

# Liquid-phase-infiltration of EB-PVD-TBCs with ageing inhibitor

B. Saruhan [a,*], A. Flores Renteria [a], M. Keshmiri [b], T. Troczynski [b]

[a] *German Aerospace Center (DLR), Institute of Materials Research, Cologne, Germany*
[b] *University of British Columbia, Department of Metals and Materials Engineering, Vancouver, Canada*

Received 20 June 2004; received in revised form 20 October 2004; accepted 29 October 2004
Available online 13 June 2005

**Abstract**

Partially yttria stabilized zirconia (PYSZ) is the state-of-the-art material for current thermal barrier coating (TBC) applications at aircraft engines. It introduces intrinsic properties leading to increased lifetime of superalloy turbine blades and engine efficiency. The new generation turbines generate higher gas temperatures, which seriously affects the thermal stability of the state-of-the-art TBC materials, mainly because of considerable phase transformation- and/or sintering-induced volume changes. These processes cause degradation of columnar microstructure of electron-beam physical vapor deposited (EB-PVD) coatings and raise modulus of elasticity and as a result, the internal stresses. One of the suggested strategies for the improvement of sintering resistance is to infiltrate TBCs with another oxide. This aims to reduce the diffusion rate at the nano-structured feather-arm features and to avoid inter-columnar pore closure.

This paper deals with infiltration of EB-PVD PYSZ-structures with a liquid-phase precursor based on alumina and titania to inhibit sintering. After heat-treatment of infiltrated coatings at 1000 and 1100 °C, microstructure is characterized by SEM/EDX and compared with as-coated state-of-the-art material aged under same conditions. The mechanism, which may stop or inhibit the sintering at TBCs is discussed. Attributions to the thermal stability and the potential use of the infiltration technique in EB-PVD-coatings are addressed.


*Keywords:* $TiO_2$; $Al_2O_3$; $ZrO_2$; Thermal barrier coating

## 1. Introduction

Fuel consuming energy conversion systems can become significantly profitable by the use of ceramic-based thermal barrier coatings (TBCs) on single crystal superalloy turbine airfoils. The deposition of TBCs is employed by means of either electron-beam physical vapor deposition (EB-PVD) or by air plasma spraying (APS).[1,2] The state-of-the-art material for such TBCs is partially yttria stabilized zirconia (PYSZ) which exhibits intrinsically outstanding properties such as low thermal conductivity, low Young's modulus, and relatively high thermal expansion coefficient.[3] These essential properties are impaired during service in turbines because of high gas temperatures exceeding 1250 °C and prolonged service durations which exceed generally 10,000 h.[4]

The most challenging mechanisms affecting the usage of EB-PVD PYSZ TBCs refer to phase stability and sintering which are associated with an increase of Young's modulus and the thermal conductivity. As a consequence, these property changes lead to shorter lifetime for the TBC coatings and detrimental results in turbine blades.[5,6] The conditions will worsen when the gas inlet temperature of new generation gas turbines exceeds 1600 °C in order to obtain higher turbine efficiency. Thus, the surface temperature in airfoils will increase as high as 1350 °C, resulting in a higher tendency to sintering and subsequently to other detrimental property changes.[7–9]

As-coated EB-PVD PYSZ layers consist of single crystalline columns, which are weakly interconnected and display open porosity. The gap between the columns can be larger at the coarser surface region and narrower at submicron sized finer columns at the root area near to substrate side of the coating. The distribution and proportion of the porosity at the EB-PVD TBCs are mainly controlled by

* Corresponding author.
*E-mail address:* bilge.saruhan@dlr.de (B. Saruhan).

0955-2219/$ – see front matter © 2004 Elsevier Ltd. All rights reserved.
doi:10.1016/j.jeurceramsoc.2004.10.024

deposition parameters. The open porosity at the column edges is built by secondary shadowing during the growth of the nano-structured feather-arms.[1,10] Due to the interruption of deposition on rotation during coating process, there occurs intra-columnar porosity of a lower volume fraction within each column. Inter-columnar gap and feather-arm features are count for open porosity whereas intra-columnar porosity for closed porosity.

As the service temperature increases, inter-columnar gap may close occasionally at the connection points leading to an increase in elasticity modulus and to a reduction of the strain compliance of the coating. This contributes to failure of the TBC coating system. Ideally, the in-plane spaces between the columns should practically remain unchanged at higher temperatures as the columns are fixed to the fully dense substrate and to the thermally grown oxide (TGO).

Previous studies conclude that open porosity is more susceptible to sintering related pore closure, while the changes in finer intra-columnar closed porosity are driven by pore diffusion and pore growth.[11,12] It is assumed that mainly the pore closure is what leads to an increase in thermal conductivity and Young's modulus of TBCs.

Due to the complex morphological built of the EB-PVD TBCs, it is difficult to define the sintering-related mechanisms and their influence on thermal property changes. Temperature-induced sintering is a kinetically activated process and may be due to the lattice, volume or surface diffusion mechanism. It is likely that several material transport mechanisms occur simultaneously and contribute concurrently to property deterioration in EB-PVD TBCs.

Production of sintering-resistant EB-PVD TBCs by modifying the coating chemistry, composition, and crystal structure is under investigation.[13–16] Nevertheless, the advantageous properties of well established PYSZ TBCs such as low conductivity and Young's modulus can be further used if the sintering resistance is improved by sheathing the column surfaces with a nanometer scale layer of sintering inhibitor. Successful sintering inhibiting material should not bridge the gap between the columns. Instead, the feather-arm secondary column surfaces should be coated homogeneously with nano-scale layer of the sintering inhibitor material.

The morphological differences in TBCs created by altering the process parameters are the shape of the primary columns, shape and size of the so-called feather-arm structured secondary columns, and shape and size of the closed pores.[1,17–19] Most of the pores within the primary columns and the feather-arm secondary columns are anisotropic, while some of the intra-columnar round pores are isotropic in shape.[1,17–20] The surface area change of the open and closed porosity has potentially significant influence on the kinetic of sintering process. The analysis of the contribution of each pore family (feather-arm secondary columns, intra-, and inter-columnar pores) to thermal insulating capabilities of TBCs would provide a guideline for engine manufacturers for designing more reliable coatings with optimized thermal properties by controlling the manufacturing process variables. This would save tremendous time and effort in achieving efficient turbine engines.

Many innovative methods are reported for precise and detailed evaluation of the changes in open and closed porosity during annealing of TBCs by means of X-ray and neutron scattering.[19–24] These methods are based on transmission of X-ray or neutrons through the geometry or cross-section of TBCs and yield an extensive quantitative evaluation of the sintering process.

As to the prevention of sintering in TBCs, oxides such as titania, hafnia or alumina are suggested as attractive sintering inhibitors since these neither form any binary compound nor yield an eutectic with zirconia.[25,26] It is postulated that a sheathing layer of unstabilized zirconia or hafnia may sinter or bond together during high temperature treatment. However, since these bonds may break upon cooling through a disruptive tetragonal to monoclinic transformation, the concept is attractive for TBCs of aircraft engines that have short thermal cycles.[26] For land based power generating engines with longer operating cycles, other oxides such as alumina are suggested due to their inertness towards TBC column material, PYSZ.[25]

By immersion of the as-coated EB-PVD TBCs in a chemically processed low viscosity sol bath (i.e., metal alkoxides), formation of an extremely thin nano-sized layer on the outer surfaces of fine feather-arm features may be achieved by infiltration, wetting and gelation of the sol. The sol penetrates in the gaps within adjacent columns and wets the feather-arm surfaces without filling them. If the inter-columnar gap is filled by sintering inhibiting material, this may increase the bonding of adjacent columns as well as enhance sintering of the feather-arm feathers to each other, reducing inter-columnar porosity and consequently increasing the thermal conductivity of EB-PVD TBCs.[26]

This paper describes the method for post-infiltration of EB-PVD coated PYSZ TBCs with alumina and titania sols. The applicability of these two candidate materials as sintering inhibitor is evaluated. The results related to the sintering resistance of post-infiltrated EB-PVD TBCs at 1000 and 1100 °C are compared with that of as-coated TBC material. Discussion based on wetting and/or gap-filling processes for suggested sintering inhibitor materials during post-infiltration are made. The diffusion mechanisms in the vicinity of infiltrated material and the EB-PVD TBCs are addressed.

## 2. Materials and methods

### 2.1. Electron-beam physical vapor deposition

For the EB-PVD processing of the coatings, pilot plant equipment ESPRI (von Ardenne, Germany) with a maximum EB-power of 150 kW was used. The substrates were both metallic and dense alumina plates. During the deposition process the average substrate temperature was adjusted to $975 \pm 25$ °C. The ingot source material was bottom fed

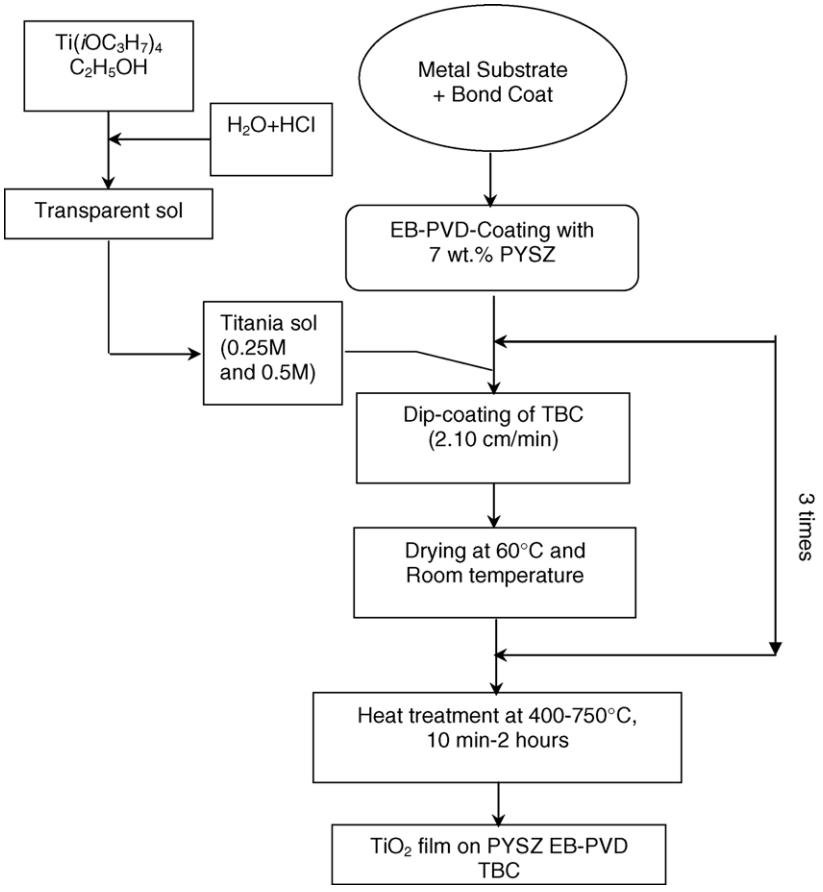


Fig. 1. Flow chart showing the sol preparation route for titania and describing the post-infiltration process of the EB-PVD coated samples with this sol.

in a water-cooled copper crucible for evaporation. The electron beam power on the source was equilibrated to 70 kW during deposition at constant focus and beam pattern conditions by keeping a constant evaporation rate. The substrates were rotated during coating. A controlled amount of oxygen was bled into the deposition chamber in order to maintain a stoichiometric oxygen composition in the coating.

### 2.2. Sol preparation and infiltration of TBCs

Alcohol-based titania and alumina sols were prepared as indicated in the flow charts shown in Figs. 1 and 2. The precursor for the titania sol was titanium tetra-*iso*-propoxide Ti($i$OC$_3$H$_7$)$_4$ (97%, Aldrich) and for the alumina sol aluminum *iso*-propoxide [Al(iOCH$_3$)$_3$] in alcohol solution. Titania sol was mixed with ethanol ($C_2H_2O_5$) and then hydrolyzed by drop wise addition of double distilled ionized water and concentrated HCl to the mixture. The solution was stirred for 30 min at 25 °C followed by ageing under static condition for 20 h as stored in a closed container to obtain a transparent sol. Titania sol has been prepared in two concentrations, 0.25 and 0.5 M which are designated in the following text as 0.25 M-titania sol and 0.5 M-titania sol.

Alumina sol was hydrolyzed by addition of 3 l distilled water to yield a solution of 0.5 M. By addition of 1 M $HNO_3$,

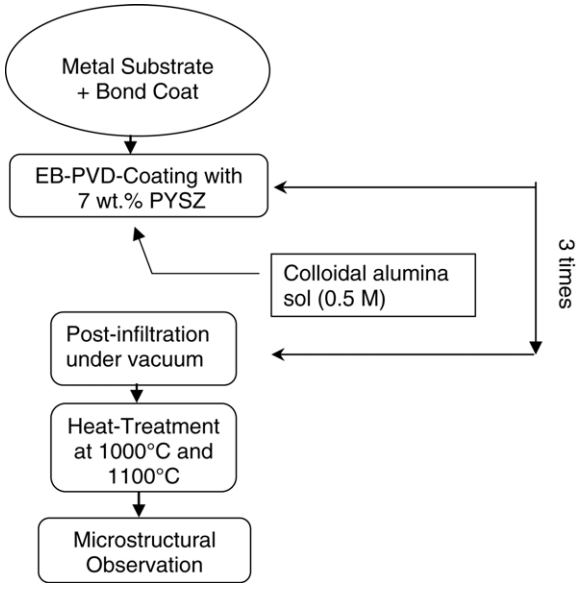


Fig. 2. Flow chart showing the route for post-filtration of EB-PVD-TBCs with alumina sol.

the solution of pH is adjusted to 4. Under vigorous stirring for 16 h at 85 °C, a colloidal sol was obtained.

Infiltration of the EB-PVD coated TBCs were carried out by embedding the samples in these sols under vacuum and by withdrawing samples with a speed of 2.1 cm/min after the completion of infiltration. The dip-coated TBCs were dried at 60 °C overnight and then heat-treated at 750 °C for 20 min to convert the sol to ceramic (see Figs. 1 and 2).

### 2.3. Characterization methods

As-coated and post-infiltrated TBCs were characterized microstructurally and compositionally by using scanning electron microscopy (SEM) and energy dispersive X-ray spectroscopy (EDS) (LEITZ LEO 982 microscope, Germany). Other compositional determinations are carried out by using an X-ray Fluorescence Analyzer (Oxford MESA 5000, Germany). TBCs in the as-coated and annealed condition are evaluated by Brunauer–Emmett–Teller (BET) gas absorption method to obtain the surface area values as detailed in.[27]

## 3. Results

After post-infiltration and heat-treatment, the microstructure and composition of TBC samples were analyzed by SEM and EDX. The results of these analyses for alumina post-infiltrated TBCs are shown in Fig. 3 and for titania post-infiltrated TBCs in Fig. 4.

Table 1
EDS spot analyses measured 20 and 170 μm distance from the tip of the columns display poor infiltration with alumina sol

| Distance from column tip (μm) | Al (at.%) | Zr (at.%) | Si (at.%) | O (at.%) |
|---|---|---|---|---|
| 20 | 10.49 | 34.69 | 6.10 | 48.72 |
| 170 | None | | None | |

SEM/EDS analysis shown in Fig. 3 and Table 1 display that the post-infiltration of TBCs with 0.5 M alumina sol results in lack of coverage at the feather-arm features. Instead, it was observed that the inter-columnar gaps are filled with nano-sized particles of alumina. Moreover, the infiltration depth is limited with 20 μm (Table 1). Alumina sol coats the column tips of the TBC with a thick layer, and thus, hinders infiltration of the sol further down in the gaps between the columns. As a result, no alumina was found by EDS-analysis at a distance of 170 μm from the column tip (Fig. 3 and Table 1).

Fig. 4 demonstrates that the post-infiltration process with titania sol yields mostly a thin layer of titania at the column edges of feather-arm features. However, a bonding coverage of more than one feather-arm tips was not prevented (Fig. 5). Titania sol is prepared in two concentrations; 0.25

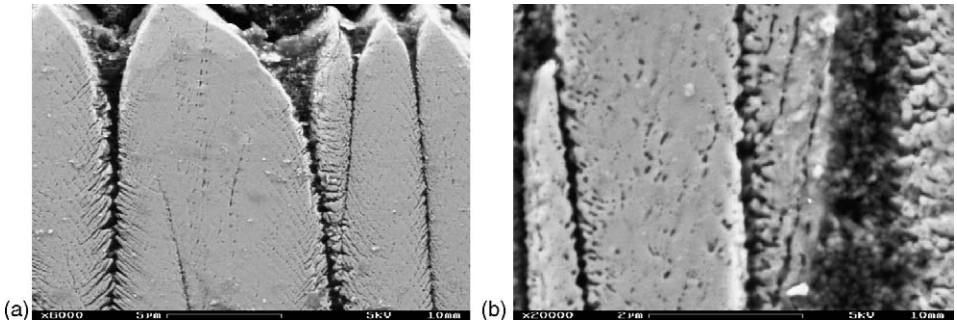


Fig. 3. Scanning electron images of the 0.5 M $Al_2O_3$-infiltrated PYSZ EB-PVD-TBCs after 1 h of ageing at 1000 °C: (a) from the tip of the coating and (b) at the substrate side of the coating.

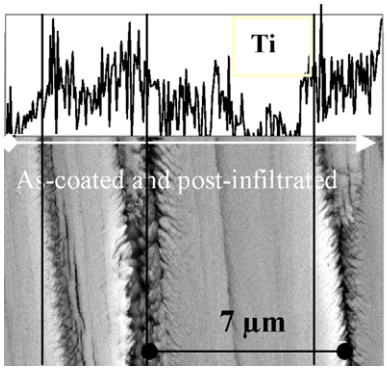


| Distance from column tip | Ti atm.% | Zr atm.% | O atm.% |
|---|---|---|---|
| 50 μm | 1.5 | 26.5 | 72.0 |
| 70 μm | 0.9 | 28.7 | 70.4 |
| 100 μm | 0.6 | 27.1 | 72.3 |
| 190 μm | 0.2 | 26.9 | 72.9 |

Fig. 4. Scanning electron image of 0.25 M-titania sol post-infiltrated PYSZ EB-PVD coating shown with corresponding Ti-EDS line scan above. In contrary to the alumina sol, Ti is detectable at a distance of 190 μm from the column tip (total coating thickness 200 μm). The amount of Ti decreases gradually from top to bottom of the EB-PVD coating.

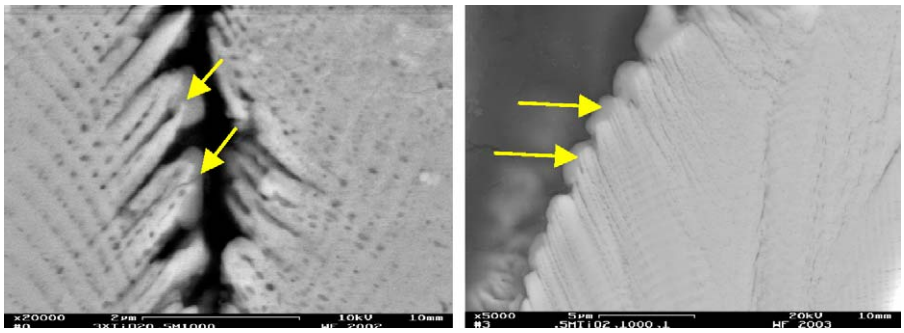

Fig. 5. Scanning electron images of titania post-infiltrated PYSZ EB-PVD-coating. The arrows point out the bonding coverage of the feather-arm edges by titania-sol.

and 0.5 M. The grade of the infiltration weakens for both sol concentrations towards the bottom of the approximately 200 μm thick EB-PVD coating (see table in Fig. 4 for 0.25 M-titania). EDS-analysis of the 0.5 M-titania infiltrated TBC at 5, 30 and 170 μm distance from the coating surface shows that the amount of Ti decreases from 6.66 to 1.88 at.%.

After infiltration of TBCs with titania sols and ageing up to 1100 °C with various intervals, the TBCs are investigated microstructurally and their microstructure is compared with that of the non-infiltrated TBCs (Fig. 6). The higher sol concentration yields a thicker layer of titania at the TBC-coating tip, due to the increase in sol viscosity.

After ageing for 20 min at 1000 °C, a very slight change in the morphology is observed for all titania post-infiltrated coatings. No visible difference was observed between the as-coated and post-infiltrated TBCs. It is most likely that, at this stage, a decrease of the intra-columnar surface area occurs. After 1 h of ageing at the same temperature, however, an intensive intra-columnar pore closure combined with the reduction of voids at the feather arms is observed which results in broadening of these features. Although, these processes take place at the non-infiltrated and titania post-infiltrated TBCs, the column-edge porosity of titania sol post-infiltrated TBCs seem to be slightly better maintained on prolonged high temperature exposure. Notably, inter-columnar bridging is more promoted with higher sol concentration (0.5 M-titania).

In order to determine the chemical interaction between infiltrated titania and the PYSZ column material, EDS analysis are carried out. Fig. 7 shows the line scan EDS-analysis at the tip region of 0.5 M titania post-infiltrated PYSZ column after 5 h of ageing at 1100 °C. According to this analysis, the intensity of Ti in the PYSZ-area becomes null, whereas Zr-intensity in titania area lies around 3 elmt.%.

To quantitatively analyze that, EDS spot analysis with a distance of 2 μm on both sides of the PYSZ/$TiO_2$-interface have been carried out after ageing the coatings for 1, 5 and 100 h at 1000 °C and 5 h at 1100 °C. Fig. 8 demonstrates the positions of the EDS spot analysis. The analyzed distance is chosen as 2 μm in order to avoid any contribution of zirconia or titania which may come from that beneath the surface. The results obtained from the spot analysis are given in Table 2 and show that the amount of zirconia in titania area increases with the ageing time. Exposure times longer than 5 h do not increase the amount of diffused zirconia in titania. The maximum detected Zr-content is 14 at.%. No significant difference is observed by increase of ageing temperature from 1000 to 1100 °C.

Table 2
Results of EDS-analysis of the 0.5 M-titania post-infiltrated EB-PVD TBC after 1 h, 5 and 100 h ageing at 1000 °C and 5 h ageing at 1100 °C

| Annealing conditions | Ti (at.% in $ZrO_2$) | Zr (at.% in $TiO_2$) | Y (at.% in $TiO_2$) |
|---|---|---|---|
| 1000 °C, 1 h | 0.79 | 10.22 | 0.91 |
| 1000 °C, 5 h | 0.82 | 14.55 | 0.92 |
| 1000 °C, 100 h | 0.94 | 14.20 | 1.90 |
| 1100 °C, 5 h | 1.00 | 14.55 | 1.10 |

Composition is given at a distance of 2 μm at each side of the PYSZ/$TiO_2$-interface.

## 4. Discussion

Sintering process as evaluated for spherical particles goes over three main steps: initial, intermediate and final stages.[28,29] There are five possible diffusion mechanisms which can occur during sintering. Among those, only the evaporation–condensation mechanism results in shrinkage during initial stage. Despite the occurrence of surface area reduction, which consequently reduces the amount of open porosity, at the initial stage of sintering, the surface and lattice diffusion mechanisms yield no shrinkage. Sintering-related volume reduction occurs mainly at the intermediate stage resulting in shrinkage and increase of local density. Pore diffusion and consequently pore growth occur at the final stage of sintering, which results in the formation of larger pores at the expense of fine and homogeneously distributed ones.

Many of the important effects of surface area reduction arise from the fact that surface energy changes bring about a pressure difference across a curved surface.[29] In TBCs, such surfaces are due to the positive and negative curvatures around feather-arms as well as at the capillaries created due to the space between the feather-arms. When a surface is not spherical, as it is the case of nano-sized feather-arms of EB-

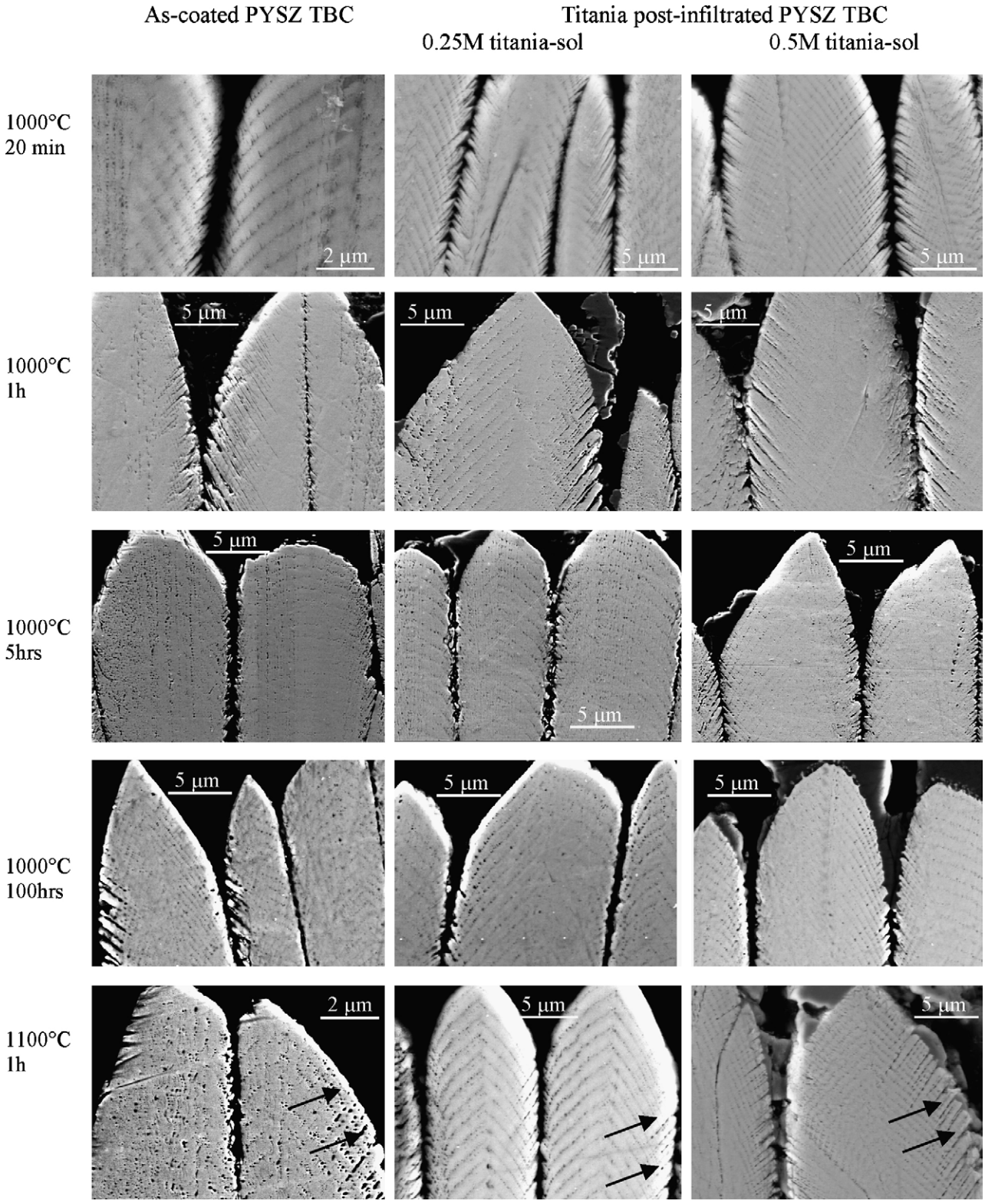


Fig. 6. Scanning electron images of the as-coated (left) with 0.25 M (middle) and 0.5 M (right) titania sol post-infiltrated PYSZ TBCs after annealing at 1000 °C for 20 min, 1, 5, and 100 h and at 1100 °C for 1 h.

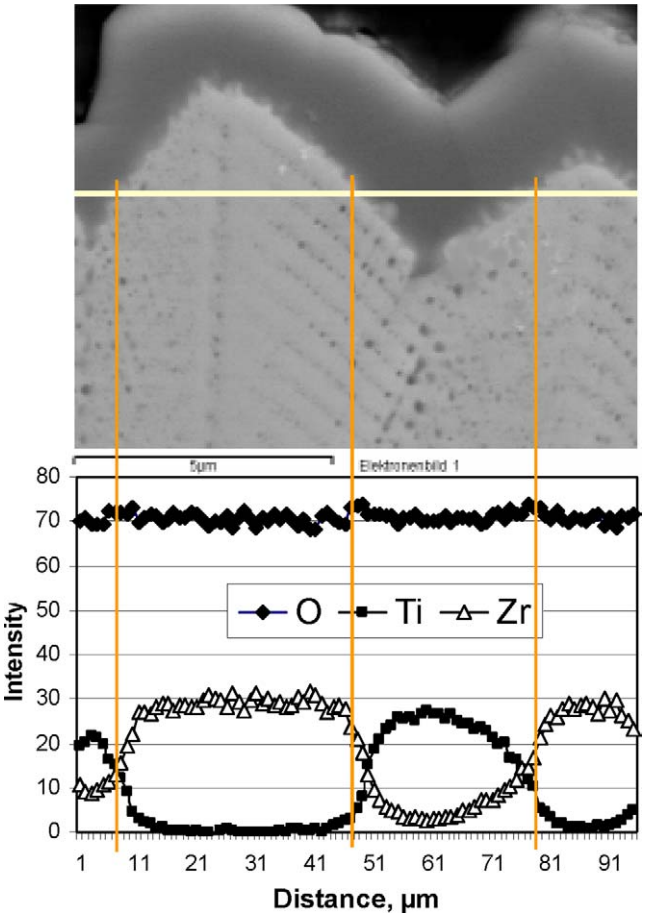


Fig. 7. EDS Line scan-analysis at the tip of 0.5 M-titania post-infiltrated EB-PVD PYSZ TBC after 5 h ageing at 1100 °C.

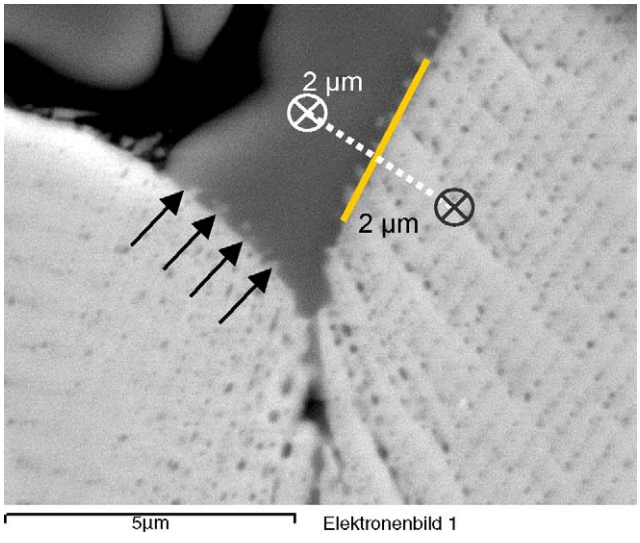


Fig. 8. Scanning electron image of the 0.5 M-titania post-infiltrated EB-PVD PYSZ TBC at the tip region showing the positions of the EDS spot analysis (Table 2). Note some loose light grey $ZrO_2$ particles within the titania area at the post-infiltrated TBCs after ageing for 5 h at 1100 °C.

PVD TBCs, the pressure difference can be expressed with the principal radii of the curvature. It is this pressure difference, which determines the rate of sintering.

Matter transport and re-condensation of the transported material at a more concave surface leads to aspect ratio changes and is controlled by changes in surface energy, vacancy concentration and activation energy, as well as by pressure difference. Also, a contribution of material transport from the bulk to the surface over lattice diffusion is likely. Although it is not clearly defined, it appears that the process, which takes place prior to the volume-related sintering process is the growth of intra-columnar pores at the expense of finely distributed closed porosity. This process results in a form change of the porosity and affects very little the change in total surface area. By accumulation of many small pores through pore diffusion mechanism, larger and rounder pores form within the columns of EB-PVD TBCs. Greatest surface area changes are due to the changes in open porosity. EB-PVD TBCs in the as-coated state display high population of nano-sized open porosity (i.e., feather-arms) which originates from competitive growth and shadowing during vapor deposition.[10] These features yield a substantial open porosity related surface area due to the voids between the feather-arms. As the temperature increases above 1000 °C, the specific surface energy reduction becomes dominating and leads to the reduction of the space between the feather-arm features, bringing them into contact and subsequently to matter transport at the contact points. As a follow-up, the aspect ratio of these feather-arms (i.e., secondary columns) is reduced.

The BET measurements on the as-coated and aged PYSZ EB-PVD TBCs exhibit that the annealing temperature and time play an important role on the reduction of the specific surface area. A comparison of the surface area results obtained by BET measurements at the temperature range between 700 and 1100° reveals a significant specific surface area reduction starting already at 900 °C, summing up to a pore surface area reduction of 50% after one hour at

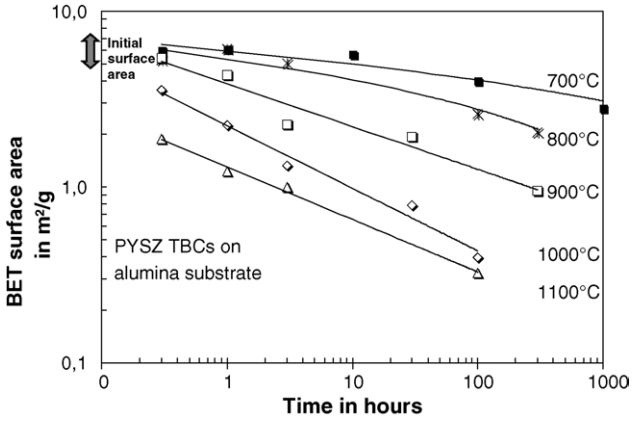


Fig. 9. Surface area reduction versus time curves of as-coated EB-PVD PYSZ TBCs at the temperature range of 700–1100 °C.

1100 °C (see Fig. 9). The major change in sintering rate occurs at about 1000 °C. This agrees well with the results from previous studies which report the highest sintering rate between 900 and 1100 °C for one hour exposure time.[11,12] Since the driving force for sintering is the surface energy reduction, this rate change is presumably due to partial stabilization of the process kinetics relating to the morphology changes at the pore surface. Alternatively, it can be suggested that this rate change is due to a change in the sintering mechanism. As mentioned above, the surface area reduction is a result of pressure differences between solid/vapor-interfaces related to the surface curvature differences at the solid/vapor walls. During the re-arrangement of surfaces by change in surface energy, a diffusion-activated process may follow and this certainly shows another kinetic.

Matter transport (e.g., from the surface with high curvature differences to more stable spherical surface) which may be attributed to the occurrence of surface diffusion mechanism occurs at 900 °C after approximately 5 h, whereas at 1100 °C already within 30–40 min. It is likely that this is when the aspect ratio change of the feather-arm secondary columns takes place.

Before claiming any improvement in sintering resistance of post-infiltrated TBCs, it is necessary to note that EB-PVD TBCs contain at least two different sorts of porosity (i.e., inter and intra-columnar). Up to date it has not been clearly verified which order exists in the occurrence of pore closure and matter transfer at these two different types of porosity. By infiltration of a TBC, one achieves only a surface coverage of the column edges. Therefore, it is anticipated that this method cannot directly affect the sintering process involving the intra-columnar porosity. According to this argumentation, our observations regarding the sintering inhibition have principally concerned the changes in the open porosity at the feather-arms.

Considering the experimental results, we postulate that the infiltration of EB-PVD TBCs with alumina sol is ineffective in terms of inhibition of the ageing process. Alumina sol fails to coat the feather-arm nano-structures of EB-PVD TBCs. Instead it fills the gap between the columns. The inter-columnar space compensates for thermal expansion mismatch between the coating and the substrate, and thus, introduces excellent thermal shock resistance to these coatings. Therefore, its presence as well as its upholding during service is of importance. The surface energy reduction at the voids of feather-arm structures is not impeded by the presence of alumina at the inter-columnar gap, instead a more deleterious ageing takes place already after 1 h at 1000 °C (see Fig. 3). This is probably because of the colloidal type of alumina sol used in this study. Colloidal sols contain nano-sized hydrolyzed particles which yields poor or no wetting of the surfaces, especially when they are not horizontal and show different curvatures as in the case of TBCs. Nano-particles percolates almost on the column tips and sets a thick layer between the column edges which then stops the infiltration of the sol in the depth of the coating.

Infiltration of EB-PVD TBCs with titania sol, in contrast, provides a visible wetting of the feather-arm features by the titania sol. On immersion of the as-coated EB-PVD TBC in low viscosity titania sol, the sol penetrates into the gaps between the adjacent columns and wets the feather-arm surfaces. As a result, a nanometer size film forms. SEM observations show that the post-infiltration process yields mostly a thin titania layer at the edges of the feather-like secondary columns which is expected to trap the diffused $Zr^{4+}$ ions during ageing. In some areas, however, due to the insufficient wetting of secondary columns by titania, secondary column bridging has also been observed (see Fig. 5). In the case that the inter-columnar gaps are filled by the sol and titania clusters are formed around the feather-arm tips, bridging or bonding of the adjacent secondary columns may occur. These lead to coarsening as well as shortening of the feather-arm regions resulting in more deleterious effects.

It has been suggested in recent patents that oxides such as alumina and titania are attractive candidates as sintering inhibitor for EB-PVD TBCs since they are chemically inert towards zirconia up to certain concentration levels.[25,26] Titania forms no binary phase with zirconia. Instead, the $TiO_2/ZrO_2$-phase diagram indicates formation of solid solutions at both oxide sides.[30] The studies carried out on plasma-sprayed $ZrO_2$–$Y_2O_3$–$TiO_2$ coatings reported the formation of higher concentrations of $t$-$ZrO_2$ than that in equivalent $ZrO_2$–$Y_2O_3$ coatings[31,32]. Especially at higher $TiO_2$—contents such as 18 wt.%, no $t \rightarrow m$ transformation was observed in the as sprayed coatings. After quenching from temperatures higher than 1200 °C, the plasma-sprayed coatings showed an increased relative concentration of $t'$-$ZrO_2$. For high titania concentrations, $TiO_2/ZrO_2$-phase diagram predicts no cubic-$ZrO_2$ formation[33]. Addition of $TiO_2$ apparently increases the stability field of $t'$-$ZrO_2$. Otherwise for lower $TiO_2$-concentrations, decomposition of $t'$-$ZrO_2$[32] or conversion to $c$-$ZrO_2$[33] depending on heat-treatment conditions have been reported. Regarding these, one has to consider the compositional changes at the PYSZ TBCs after titania infiltration.

As the EDS-analysis at the column-tip region shows, Zr diffuses into the infiltrated titania areas and probably forms a titania solid solution. EDS-results of Table 2 show that the segregation of Zr into the titania areas starts already at lower temperatures after relatively shorter exposure times. The highest measured concentration is 14 at.%, which remains constant even after 100 h of exposure at 1000 °C, indicating a saturation limit for zirconia. This may be the reason why one observes some Zr-particles within the titania areas after ageing. Yttrium shows a similar trend as zirconia. Ti, however, diffuses almost in a negligible amount into zirconia (Fig. 7 and Table 2). This behavior indicates higher diffusion rates for Zr and Y than Ti. On saturation of this solid solution, a condensation of Zr in the concave curvature areas of the feather arms may occur. Occurrence of this phenomenon can provide a more effective hindrance of sintering. The requirement to achieve this condition is an optimum deposition of nano-

sized thin layer of titania around PYSZ secondary columns by infiltration.

After 5 h ageing at 1100 °C, segregation of $Zr^{4+}$ ions within the titania phase is detected in the post-infiltrated TBC. At a distance of 2 μm behind the $TiO_2$/PYSZ-interface, up to 14 at.% Zr in titania has been found by EDS-analysis (Fig. 8, Table 2). If we consider that the space between feather-arm secondary columns is approximately 100–200 nm and the distance for the $Zr^{4+}$ ions segregation and hence an order of magnitude smaller than the distance of 2 μm in that Zr was found within titania. It can be concluded that when the titania infiltration leads to cluster formation around the feather-arms, then it is likely that feather arms will be bonded together and this provides almost a bridge for Zr-diffusion from one secondary column to the other. In such case, the sintering at EB-PVD TBCs will not be inhibited, but promoted. Taking these facts into account, it is the principal requirement that the post-infiltration of the PYSZ EB-PVD TBC columnar structure with $TiO_2$ yields an extremely thin and continuous covering layer. Any divergence from this requirement leads to deleterious effects in reduction of sintering rate in EB-PVD TBCs.

The other concern is whether or not the infiltration of TBCs with titania has any influence on the intra-columnar pore closure. In other words, it is not clear if obstruction of Zr-diffusion by trapping it at the thin infiltrated titania layers slows down the intra-columnar pore diffusion. Pore diffusion is to be likely driven by lattice or bulk diffusion of zirconia and presumably it occurs in the opposite direction of the bulk matter transfer. By considering the fact that the titania infiltrated EB-PVD TBCs display a higher intra-columnar pore population even after 1 h of ageing at 1100 °C, we assume that the influence of infiltration of TBCs with titania extends over the surface related matter and affects the intra-columnar porosity. Increase in the size of the closed porosity after 1 h of ageing at 1100 °C is another indication of a pore diffusion stimulated pore growth.

## 5. Conclusion

Alumina sol infiltrated EB-PVD coatings exhibit no resistance to ageing at service temperatures. Titania sol-infiltration of EB-PVD coatings yields titania layers thinner than 100 nm at feather-arm features. However, the distribution of titania layer is not homogeneous and partial clustering around the feather-arm secondary columns results in bridging and bonding.

For as-coated and titania sol post-infiltrated coatings, it can be anticipated that the increase in ageing temperature and prolongation of exposure time lead to considerable reduction of feather-arm lengths as well as the decrease of the void between the feather-arms resulting in lower aspect ratios and broadening of the nano-structured feather-arm features. Titania infiltration does not lead to a significant difference in terms of maintenance of open porosity. It is however likely that the infiltration with titania sol might suppress the pore diffusion and growth since a considerable amount of left fine intra-columnar porosity in the post-infiltrated coatings is observed. In order to achieve fully satisfactory results, it is necessary to deposit a titania layer thinner than 10–20 nm very homogeneously around the secondary columns.

## References


1. Schulz, U., Fritscher, K. and Leyens, C., Two-source jumping beam evaporation for advanced EB-PVD TBC systems. *Surf. Coat. Technol.*, 2000, **133–134**, 40–48.
2. Zhu, D. and Miller, R. A., Sintering and creep behavior of plasma-sprayed zirconia- and hafnia-based thermal barrier coatings. *Surf. Coat. Technol.*, 1998, **108–109**, 114–120.
3. Leyens, C., Schulz, U. and Peters, M. Advanced thermal barrier coatings systems: research and development trends. In *High Temperature Coatings-Science and Technology IV*, ed. N. B. Dahotre, J. M. Hampikian and J. Morral. TMS, Warrendale, PA, 2001, pp. 62–76.
4. Leyens, C., Schulz, U., Bartsch, M. and Peters, M., R&D status and needs for improved EB-PVD thermal barrier coating performance. In *MRS Fall Meeting 2000, Vol. 645E*, Mater. Res. Soc. Symp. Proc., 2001, pp. M10.1.1–12.
5. Schulz, U., Leyens, C., Fritscher, K., Peters, M., Saruhan-Brings, B., Lavigne, O. *et al.*, Some recent trends in research and technology of advanced thermal barrier coatings. *Aerospace Sci. Technol.*, 2003, **7**, 73–80.
6. Schulz, U., Fritscher, K., Leyens, C. and Peters, M., The thermocyclic behavior of differently stabilized and structured EB-PVD TBCs. *JOM-e*, 1997, **49**(10), 2.
7. Zhu, D., Miller, R. A., Nagaraj, B. A. and Bruce, R. W., Thermal conductivity of EB-PVD thermal barrier coatings evaluated by a steady-state laser heat flux technique. *Surf. Coat. Technol.*, 2001, **138**, 1–8.
8. Wang, Z., Kulkarni, A., Desphande, S., Nakamura, T. and Herman, H., Effects of pores and interfaces on effective properties of plasma sprayed zirconia coatings. *Acta Mater.*, 2003, **51**, 5319–5334.
9. Wellman, R. G. and Nicholls, J. R., On the effect of ageing on the erosion of EB-PVD TBCs. *Surf. Coat. Technol.*, 2004, **177–178**, 80–88.
10. Schulz, U., Terry, S. G. and Levi, C. G., Microstructure and texture of EB-PVD TBCs grown under different rotation modes. *Mater. Sci. Eng. A*, 2003, **360**, 319–329.
11. Fritscher, K., Schulz, U., Leyens, C. and Peters, M., Aspects on sintering of EB-PVD TBCs. In *Ceramic Materials and Components for Engines*, ed. J. G. Heinrich and F. Aldinger. Wiley-VCH, 2001, pp. 517–522.
12. Schulz, U., Fritscher, K., Leyens, C. and Peters, M., High-temperature aging of EB-PVD thermal barrier coatings. *Ceram. Eng. Sci. Proc.*, 2001, **22**(4), 347–356.
13. Saruhan, B., Schulz, U., Vassen, R., Pracht, G., Bengtsson, P., Friedrich, C. *et al.*, Evaluation of two new thermal barrier coating materials produced by APS and EB-PVD. *Ceram. Eng. Sci. Proc.*, 2004, **25**, 363.
14. Matsumoto, M., Yamaguchi, N. and Matsubara, H., Low thermal conductivity and high temperature stability of $ZrO_2$–$Y_2O_3$–$La_2O_3$ coatings produced by electron beam PVD. *Script. Mater.*, 2004, **50**(6), 867–871.
15. Nicholls, J. R., Lawson, K. J., Johnston, A. and Rickerby, D. S., Methods to reduce the thermal conductivity of EB-PVD TBCs. *Surf. Coat. Technol.*, 2002, **151–152**, 383–391.

16. Saruhan, B., Francois, P., Fritscher, K. and Schulz, U., EB-PVD Processing of pyrochlore-structured $La_2Zr_2O_7$-based TBCs. *Surf. Coat. Technol.*, 2004, **182**, 175–183.
17. Schulz, U., Münzer, J. and Kaden, U., Influence of deposition conditions on density and microstructure of EB-PVD TBCs. *Ceram. Eng. Sci. Proc.*, 2002, **23**(4), 353–360.
18. Schulz, U. and Schmücker, M., Microstructure of $ZrO_2$ thermal barrier coatings applied by EB-PVD. *Mater. Sci. Eng.*, 2000, **276**, 1–8.
19. Long, G. G., Dobbins, T. A., Allen, A. J., Ilavsky, J., Jemain, P. R., Kulkarni, A. *et al.*, Recent developments in the characterization of the anisotropic void populations in thermal barrier coatings using ultra-small angle X-ray scattering. *Ceram. Eng. Sci. Proc.*, 2003, **24**, 517.
20. Kulkarni, A. and Herman, H., Microstructure—property correlations in industrial thermal barrier coatings. *Ceram. Eng. Sci. Proc.*, 2003, **24**, 535.
21. Kulkarni, A., Wang, Z., Nakamura, T., Sampath, S., Goland, A., Herman, H. *et al.*, Comprehensive microstructural characterization and predictive property modeling of plasma-sprayed zirconia coatings. *Acta Mater.*, 2003, **51**, 2457–2475.
22. Allen, A. J., Long, G. G., Bokari, H., Ilavsky, J., Kulkarni, A., Sampath, S. *et al.*, Microstructural characterization studies to relate the properties of thermal spray coatings to feedstock and spray conditions. *Surf. Coat. Technol.*, 2001, **146–147**, 544–552.
23. Allen, A. J., Ilavsky, J., Long, G. G, Wallace, J. S., Berndt, S. S. and Herman, H., Microstructural characterization of yttria-stabilized zirconia plasma-sprayed deposits using multiple small-angle neutron scattering. *Acta Mater.*, 2001, **49**(9), 1661–1675.
24. Ilavsky, J. and Stalick, J. K., Phase composition and its changes during annealing of plasma-sprayed YSZ. *Surf. Coat. Technol.*, 2000, **127**(2–3), 120–129.
25. Raybould, D., Strangman, T. E., Fischer, W. E. and Chipko, P. A., Thermal Barrier Coating with Alumina Bond Inhibitor, US Patent, 2000, 6,103,386.
26. Subramanian, R. and Sabol, S., Thermal Barrier Coating Resistant to Sintering, US Patent, 2001, US 6,203,927 B1.
27. Berger, L.-M., Powder and compact porous materials characterization by adsorption, In *Proc. Powder Metallurgy World Congress*, ed. J. M. Capus and R. M. German, MPIF/APMI, 1992, p. 235.
28. Kingery, W. D., Bowen, H. K. and Uhlmann, D. R., *Introduction to Ceramics* (*2nd ed.*). John Wiley and Sons, New York, 1976.
29. Kingery, W. D., Bowen, H. K. and Uhlmann, D. R., *Introduction to Ceramics*, John Wiley and Sons, New York, 1960.
30. Levin, E.M. and McMurdie, H.F., *Phase Diagrams for Ceramists*, 1975, suppl., 169, Fig. 4452.
31. Diaz, P., Ralph, B. and Edirisinghe, M. J., Transmission electron microscope characterization of a plasma-sprayed $ZrO_2$–$Y_2O_3$–$TiO_2$ thermal barrier coating. *Mater. Characterization*, 1998, **41**, 55–67.
32. Diaz, P., Edirisinghe, M. J. and Ralph, B., Microstructural changes and phase transformations in a plasma-sprayed zirconia-yttria-titania thermal barrier coating. *Surf. Coat. Technol.*, 1996, **82**, 284–290.
33. Brown, F. and Duwez, P., The zirconia–titania system. *J. Am. Ceram. Soc.*, 1954, **37**, 129–132.